Chemosphere 370 (2025) 144010

Contents lists available at ScienceDirect

Chemosphere

journal homepage: www.elsevier.com/locate/chemosphere

Insights from multiple stable isotopes (C, N, Cl) into the photodegradation of herbicides atrazine and metolachlor

Matias Levesque-Vargas [a,b], Leanne Ohlund [c], Lekha Sleno [c], Yves Gélinas [b,d], Patrick Höhener [e], Violaine Ponsin [a,b,*]

[a] Département des sciences de la Terre et de l'atmosphère, Université du Québec à Montréal, Montréal, QC, H2X 1Y4, Canada
[b] Geotop Research Centre, Montréal, QC, H2X 3Y7, Canada
[c] Département de chimie, Université du Québec à Montréal, Montréal, QC, H3C 3P8, Canada
[d] Department of Chemistry and Biochemistry, Concordia University, Montréal, QC, H4B 1R6, Canada
[e] Laboratoire Chimie Environnement, Aix-Marseille Université, 13331, Marseille, France

HIGHLIGHTS

- Photodegradation experiments on atrazine and metolachlor under simulated sunlight.
- First report of Cl isotope fractionation associated to photolysis of herbicides.
- Inverse isotope effect for Cl during atrazine direct and indirect photodegradation.
- Dual C–Cl isotope plot allows pathway identification for atrazine in surface water.
- Cl data suggest common reaction mechanism to different pathways for metolachlor.

GRAPHICAL ABSTRACT

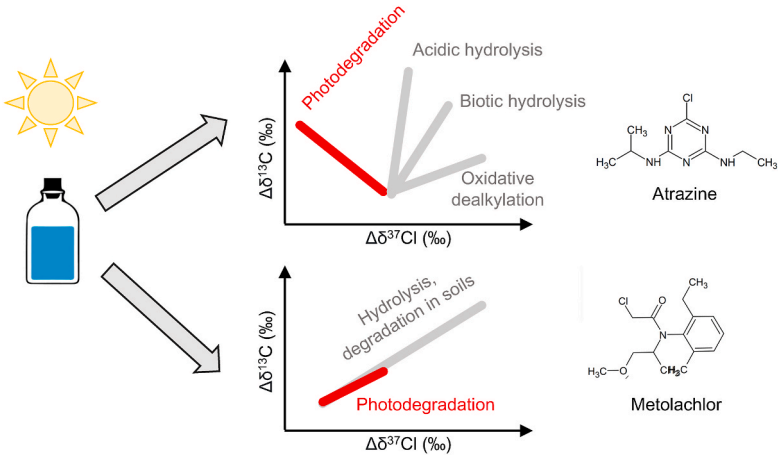

ARTICLE INFO

Handling Editor: Keith Maruya

Keywords:
Photodegradation
Isotope fractionation
Pesticides
Chlorine isotopes
Atrazine
Metolachlor

ABSTRACT

Many processes can contribute to the attenuation of the frequently detected and toxic herbicides atrazine and metolachlor in surface water, including photodegradation. Multi-element compound-specific isotope analysis has the potential to decipher between these different degradation pathways as Cl is a promising tool for both pathway identification and a sensitive indicator of degradation for both atrazine and metolachlor. In this study, photodegradation experiments of atrazine and metolachlor were conducted under simulated sunlight in buffered solutions (direct photodegradation) and with nitrate (indirect photodegradation by OH radicals) to determine kinetics, transformation products and isotope fractionation for C, N and for the first time Cl. For metolachlor, the C–Cl dual isotope slope ($\Lambda_{C/Cl}$ = 0.46 ± 0.19) is identical to previously reported values for hydrolysis and

* Corresponding author. Département des sciences de la Terre et de l'atmosphère, Université du Québec à Montréal, Montréal, QC, H2X 1Y4, Canada.
E-mail addresses: matias-lv@hotmail.com (M. Levesque-Vargas), ohlund.leanne@uqam.ca (L. Ohlund), sleno.lekha@uqam.ca (L. Sleno), yves.gelinas@concordia.ca (Y. Gélinas), patrick.hohener@univ-amu.fr (P. Höhener), ponsin.violaine@uqam.ca (V. Ponsin).

https://doi.org/10.1016/j.chemosphere.2024.144010
Received 16 October 2024; Received in revised form 16 December 2024; Accepted 20 December 2024
Available online 24 December 2024

biodegradation in soils, suggesting the same reaction mechanism (C–Cl bond breakage by SN_2 nucleophilic substitution). For atrazine, both direct and indirect photodegradation resulted in a pronounced inverse isotope effect for chlorine ($\varepsilon_{Cl} = 6.9 \pm 3.3$ ‰, and $\varepsilon_{Cl} = 2.3 \pm 1.2$ ‰, respectively), leading to characteristic dual isotope slopes ($\Lambda_{C/Cl} = -0.49 \pm 0.17$ and $\Lambda_{C/Cl} = -0.31 \pm 0.10$, respectively). These values are distinct from those previously reported for abiotic hydrolysis, biotic hydrolysis and oxidative dealkylation which are all relevant processes in surface water, opening the path for pathway identification in future field studies.

1. Introduction

Man-made organic chemicals such as pesticides are increasingly detected in groundwater and surface water worldwide and pose a major threat to ecosystems (Vijver et al., 2017) and public health (Kim et al., 2017; Evans et al., 2019). For example, exposure to the herbicide atrazine (ATR) is associated with endocrine disruption in amphibians (Tavera-Mendoza et al., 2002) and possibly birth defects in humans (Almberg et al., 2018). ATR is ubiquitous in Québec, Canada, not only in surface water but it also has been detected in drinking water (Montiel-León et al., 2019). Similarly, the frequently detected herbicide metolachlor (METO) is toxic to humans and aquatic ecosystems and is classified as a possible human carcinogen by the US EPA and the European Chemicals Agency (Agency., 2008; European Chemicals Agency, 2022). Therefore, it is necessary and urgent to unveil the processes responsible for the transformation of these contaminants in the environment to be able to predict their long-term impact on water resources (persistence, presence of transformation products-TPs) and to develop strategies to mitigate pollution.

The degradation of micropollutants in the environment often appears as a black box since many processes, that are often difficult to disentangle, can occur. In surface waters, photodegradation can substantially contribute to their overall degradation (Huntscha et al., 2008; Gerecke et al., 2001), but other processes such as biodegradation and abiotic hydrolysis can also play a major role, and the relative importance of each process is usually unknown (Fenner et al., 2013, 2021; Imfeld et al., 2021). Photodegradation can be direct (a compound absorbs photons and undergoes transformation) or indirect (a compound is transformed by energy transfer from another excited species or by reaction with very reactive, short-lived species formed in the presence of light) (Schwarzenbach et al., 2003). Such intermediates often come from dissolved organic matter (DOM excited triplet states), or nitrate (hydroxyl radicals). Indirect phototransformation is expected to be the main process for most pesticides because i) the electronic absorption spectrum of most of them shows little overlap with the spectrum of sunlight (Schwarzenbach et al., 2003), and ii) nitrate is ubiquitous in surface water in agricultural areas and it produces OH radicals that react with pesticides even at very low concentrations (Zeng et al., 2013). Indeed, previous studies have shown that photodegradation of both ATR and METO mainly occurs through reaction with OH radicals, especially in the presence of nitrate (Vione et al., 2010; Mabury et al., 1996).

Process-specific information such as isotope fractionation given by Compound-Specific Isotope Analysis (CSIA) is crucial to tease apart transformation pathways. During their transformation, molecules with light isotopes (e.g., ^{12}C) are usually degraded at a different rate than those with heavy isotopes (e.g., ^{13}C), leading to a fractionation in undegraded molecules. This approach is powerful because this fractionation helps to identify specific degradation processes when isotopes of two elements or more are monitored (Höhener et al., 2022) and quantify these processes (Aelion et al., 2009), which is extremely difficult to do with approaches relying only on concentration measurements. CSIA has been applied to characterize photodegradation of several micropollutants, such as organophosphorus pesticides (Wu et al., 2014, 2018), α-hexachlorocyclohexane (Zhang et al., 2014), bromoxynil (Knossow et al., 2020), terbutryn (Junginger et al., 2022), triclosan (Liu et al., 2020), sulfamethoxazole (Liu et al., 2024) or diclofenac (Maier et al., 2016). Most CSIA studies only monitored carbon isotopes or carbon and nitrogen isotopes because i) they are usually easier to measure and, ii) there is more literature on isotope fractionation associated to different degradation pathways for these elements. However, recent analytical advances have made chlorine isotope analysis accessible in micropollutants either by gas chromatography−single quadrupole mass spectrometry (GC-MS (Ponsin et al., 2019)), GC multiple-collector inductively coupled plasma MS (GC-MC-ICP-MS (Renpenning et al., 2018; Vinyes-Nadal et al., 2024)), or more recently by high-resolution liquid chromatography quadrupole time-of-flight mass spectrometry (LC-QTOF-MS (Prieto-Espinoza et al., 2023)). This is particularly relevant as organochlorine pesticides usually contain a high number of carbon atoms and one or two chlorine atoms, meaning that C could be affected by strong dilution of the isotope effect while this would not be the case for Cl. For example, Torrentó et al. (2021) measured a strong Cl isotope fractionation during abiotic hydrolysis of metolachlor and acetochlor, which suggests that Cl isotopes are sensitive indicators of degradation for these compounds, even if the extent of degradation is limited. For atrazine, Cl isotopes helped differentiating degradation pathways relevant under environmental conditions (e.g., acidic hydrolysis and biotic hydrolysis) that were undistinguishable with C and N data only (Torrentó et al., 2021).

As far as we know, only two studies have assessed isotope fractionation of ATR and METO during direct and indirect photodegradation: Hartenbach et al. (2008) evaluated C, N and H isotope fractionation associated to direct photodegradation of ATR with UV light (λ = 254 nm) and indirect photodegradation with OH radicals or with excited triplet states of 4-carboxybenzophenone (λ range = 308–410 nm); Drouin et al. (2021) evaluated C and N isotope fractionation associated to direct photodegradation of ATR and METO with UV light (λ = 254 nm), and under simulated sunlight (λ range = 270–720 nm), and indirect photodegradation with OH radicals, DOM or both (λ range = 270–720 nm). Contrasting C and N isotope fractionation between direct and indirect photodegradation and within each process demonstrated the influence of the choice of irradiation source on fractionation factors and therefore on the occurrence of different reaction pathways. Fractionation factors obtained for ATR and METO during indirect photodegradation with nitrate and DOM (Drouin et al., 2021) supported previous studies suggesting that indirect photodegradation is driven by OH radicals produced by nitrate in surface water impacted by agriculture. The formation of 2-hydroxy-atrazine and 2-hydroxy-metolachlor, resulting from a C–Cl bond cleavage during direct and indirect photodegradation of METO and ATR, has been reported by several studies (Torrents et al., 1997; Dimou et al., 2005; Nicol et al., 2015), which makes Cl an ideal candidate for sensitive detection of degradation and potentially identification of transformation processes.

The overall objective of this study was therefore to evaluate the sensitivity of stable Cl isotopes as indicators of photodegradation and for pathway identification for ATR and METO by providing the first data set on Cl isotope fractionation for the photodegradation of these compounds. The specific objectives were 1) to determine Cl, C and N isotope fractionation and dual-isotope slopes during direct and indirect photodegradation of ATR and METO, and 2) to assess two-dimensional isotope fractionation patterns to tease apart photodegradation from other degradation processes of these environmentally relevant pesticides for future field studies. Photodegradation experiments were conducted under simulated sunlight either in phosphate buffer (direct photodegradation) or in the presence of OH radicals generated by nitrate

(indirect photodegradation). Cl, C and N fractionation factors were derived from these experiments and TPs were monitored.

2. Materials and methods

2.1. Chemicals

Atrazine (ATR, 98% purity), metolachlor (METO, 98% purity), deethylatrazine (DEA, 98 % purity), deisopropylatrazine (DIA, 98% purity) and deisopropylhydroxyatrazine (DIAOH, 98% purity) were purchased from Toronto Research Chemicals (TRC, North York, ON, Canada). 2-hydroxy-metolachlor (METOH, 98% purity) and metolachlor ethanesulfonic acid (METO-ESA, 95.7% purity) were supplied by Dr. Ehrenstorfer (Augsburg, Germany). Metolachlor oxanilic acid (METO-OA, ≥98.0% purity), 2-hydroxy-atrazine (ATROH, 99,7% purity), and deethyldeisopropylatrazine (DEDIA, 97.8% purity) were purchased from Sigma-Aldrich (Saint-Louis, MO, USA). Internal standards used for quantification were supplied by TRC (metolachlor-d6, 97% purity), Sigma-Aldrich (atrazine-d5, ≥99.0% purity), and CDN isotopes (2-hydroxy-atrazine-d5, 99.7% purity, Pointe-Claire, QC, Canada).

2.2. Photodegradation experiments

All experiments were made in solutions buffered at pH 6.5 (28 mL of 0.1 M NaOH mixed with 100 mL of 0.1 M KH_2PO_4 in a final volume of 200 mL) to avoid acid or alkaline hydrolysis. For indirect photodegradation, $NaNO_3$ was added to the buffered solution to obtain a final concentration of 10 mg/L of NO_3^-. These buffered solutions were then spiked with ATR or METO to obtain a final concentration of 20 mg/L and 50 mg/L, respectively. Each compound was first dissolved in dichloromethane (HPLC grade) and this stock solution was added to the buffered aqueous solution under constant agitation. 24h were allowed for the DCM to evaporate and the solution to be evenly mixed.

80 mL of the final pesticide solution were transferred to 100 mL quartz tubes (Technical Glass Products, Painesville, OH, USA) plugged with a rubber cap coated with Teflon and placed in a Q-Sun Xe-1 photoreactor (Q-Lab, Westlake, OH, USA) equipped with a 1800 W Xenon lamp and a daylight Q filter simulating a summer day at noon (Q-Lab, 295–800 nm, light intensity of 0.68 Wm^{-2} at 340 nm, Fig. S1), maintained at a constant temperature of 25 °C. The lamp irradiance spectrum was regularly calibrated using a CR20 calibration radiometer (Q-Lab). 20 mL of the pesticide solution was transferred in a 60 mL serum flask and covered with aluminum foil at room temperature as controls. Experiments were made in triplicate. pH was measured at the beginning of each experiment and on an aliquot when samples were removed from the photoreactor (SenTix® 940 pH electrode, MultiLab IDS 4010-3W, YSI).

Once removed from the photoreactor, samples were transferred in serum flasks and kept frozen in the dark until further processing. 10 mL of each sample was extracted by solid-phase extraction (SPE) with 0.2 g of Sepra ZT sorbent (Phenomenex, Torrance, CA, USA) as explained elsewhere (Ponsin et al., 2019; Torrentó et al., 2019), except for samples taken toward the end of the reaction, for which most of the available volume was used for extraction. A previous study has shown that SPE does not create isotope fractionation (Torrentó et al., 2019). After SPE, eluates were evaporated to dryness and reconstituted in ethyl acetate with appropriate volumes for isotope analyses. The remaining volume of each sample was used for determining analyte concentrations.

2.3. Analytical methods

Concentrations of ATR, METO and their expected transformation products (DEA, DIA, DIAOH, ATROH, and DEDIA for ATR; METOH, METO-ESA and METO-OA for METO) were determined by high pressure liquid chromatography triple quadrupole mass spectrometry (HPLC-QqQ-MS, Nexera Series, Shimadzu, Columbia, MD, USA, coupled with a QTRAP 5500, Sciex, Concord, ON, Canada). Separation was achieved on a Zorbax Eclipse Plus C18 column (Agilent, Santa Clara, California, USA) with dimensions 4.6 × 50 mm, 1.8 μm maintained at 40 °C at a flow rate of 0.5 mL/min. The mobile phase consisted of water with 0.1% formic acid (A) and acetonitrile with 0.1% of formic acid (B). The elution gradient started with 3% B, increasing linearly until it reached 50% B at 15 min, then to 95% B at 18 min, holding at 95% B for 3 min and re-equilibration at 3% for 6 min. The MS/MS was operated in multiple reactions monitoring (MRM) mode, in both positive and negative ionization modes (MRM transitions are given in Table S1). Ion source and MS parameters were as follows: ESI voltage, 5000V in positive and −4500V in negative; source temperature, 500 °C; curtain gas, 35 psi; nebulizer and drying gases both at 50 psi. Peak integration was performed using MultiQuant™ 3.0 (Sciex), using peak area ratios of analyte/internal standard and linear regression of the calibration curve for quantitation. A standard mixture solution of ATR, ATROH and DEDIA was prepared at 0.5 μM, 0.25 μM for DEA and DIA, and 0.1 μM for DIAOH in water. A standard mixture solution of METO, METO-ESA and METO-OA was prepared at 0.5 μM, and 0,25 μM for METOH in water. A calibration curve was prepared by diluting these stock solutions in water to obtain 1, 2, 5, 10, 20, 40, 60, 80, and 100% of the above-mentioned concentrations. Internal standards ATR-d5, ATROH-d5 and METO-d6 were added to samples and calibration curve standards at 0.2 μM final concentration.

Untargeted analysis of select METO and ATR samples was performed using high-resolution HPLC-MS/MS for exact mass. A list of potential transformation products was prepared based on a literature review. Suspect-screening was made by injecting 10 μL of the samples used for concentration analysis on the same HPLC (and under the same separation conditions) coupled to a quadrupole time of flight mass spectrometer (HPLC-Q-TOF-MS, Sciex Triple TOF 5600 Concord, ON, Canada) operated both in positive and negative ion modes. The Q-TOF had an ion spray voltage of −4500V in negative mode and 5000V in positive mode and a source temperature of 450 °C. Data was analyzed using PeakView™ 2.2 and MasterView™ 1.1 (Sciex) to extract ion chromatograms of potential transformation products.

Determination of carbon isotope ratios was made with a Trace 1310 GC coupled to a Delta V Advantage isotope ratio mass spectrometer (IRMS) via a GC Isolink II interface equipped with a Pt/Ni reactor operated at 1000 °C (all from Thermo Fisher Scientific, Bremen, Germany). 2 μL of samples were injected in a large volume injector operated in split mode (split 10) at 280 °C and equipped with a Carbofrit liner (Restek, Bellefonte, PA, USA). Chromatographic separation was made on a TG-5ms column (30 m × 0.25 mm x 0.25 μm, Thermo Fisher Scientific). The oven program started at 50 °C for 1 min, increased to 250 °C at a rate of 30 °C/min, then stayed at 250 °C for 5 min. Three in-house standards (caffeine $\delta^{13}C = -32.5 \pm 0.2‰$, and two alkane mixes C12 $\delta^{13}C = -40.7 \pm 0.3‰$, and C16 $\delta^{13}C = -29.0 \pm 0.4‰$) were analyzed at the beginning of each day to ensure the stability and reproducibility of measurements, and pesticide in-house standards (Table 1) were interspersed in each sequence for referencing on the Vienna PeeDee Belemnite (VPDB) scale via a two-point calibration. Samples and standards were diluted to a similar concentration and measured in triplicate.

N isotopes in ATR were measured using the same equipment and the same GC methods as described previously for C isotopes, except that injections of 2–8 μL were performed in splitless mode and a liquid nitrogen trap after the combustion furnace eliminated the produced CO_2. Pesticide in-house standards were interspersed in each sequence. N isotopes in METO were determined following a method described elsewhere (Drouin et al., 2021). C and N isotope ratios are expressed as arithmetic means of replicate measurements with one standard deviation (±1σ). Total uncertainty for carbon and nitrogen isotopes was calculated considering uncertainties associated with sample and standard measurements.

Chlorine isotope ratios were measured following a previous study (Ponsin et al., 2019), using a 7890 B GC coupled to a 5977 B qMS

Table 1
Isotope ratios of ATR and METO in-house standards.

Compound	Standard	$\delta^{13}C \pm SD$ (‰)	$\delta^{15}N \pm SD$ (‰)	$\delta^{37}Cl \pm SD$ (‰)	Purpose
ATR	ATR_1	−26.8 ± 0.1	1.0 ± 0.1	n.d.	C and N measurements
	ATR #4	−26.4 ± 0.1[a]	n.d.	−0.9 ± 0.2[c]	Cl measurements
	ATR #11	−28.2 ± 0.1[b]	−0.6 ± 0.1[b]	3.6 ± 0.4[c]	Cl measurements
METO	MET_1	−28.1 ± 0.1	0.0 ± 0.1	n.d.	C and N measurements
	MET-I	−28.6 ± 0.1[b]	n.d.	−4.3 ± 0.2[c]	Cl measurements
	MET-F	−22.5 ± 0.1[b]	n.d.	5.1 ± 0.3[c]	Cl measurements

n.d. not determined. [a](Ponsin et al., 2019)[b](Torrentó et al., 2021)[c](Lihl et al., 2019)

(Agilent, Wilmington, DE, USA). 1 μL of sample was injected splitless in a split/splitless injector operated at 250 °C. A DB-5ms (25 m × 0.2 mm x 0.33 μm, Agilent) operated in constant flow mode (1.6 mL/min) was used for separation. The temperature program started at 60 °C (0.6 min), ramped at 33.3 °C/min to 190 °C (3 min), then 2.8 °C/min to 210 °C (3.2 min). The interface was maintained at 280 °C, the ion source at 230 °C and the quadrupole at 150 °C. Selected ion monitoring (SIM) mode was chosen for measurements and the following ions were monitored: *m/z* 200 and 202 for ATR and *m/z* 238 and 240 for METO. Samples were diluted to 10 mg/L and standards concentrations were adjusted to those of the samples with a 20% tolerance. Each sample was analyzed 10 times, and a two-point calibration was used to report isotope values (Ponsin et al., 2019). Total uncertainty for chlorine isotopes was calculated considering uncertainties (as standard error of the mean) associated with sample measurement and with the measurement of the two standards (Ponsin et al., 2019; Bernstein et al., 2011).

2.4. Evaluation of stable Isotope data

Isotopes values are reported in per mil (‰) using the delta notation (δ) relative to the international standards Mean Ocean Chloride (SMOC) for Cl, VPDB for C and air for N, following Eq. (1):

$$\delta E_{sample}(‰) = 1000 \bullet \left(\frac{R_{E,sample}}{R_{E,std}} - 1\right) \quad (1)$$

Where E is the considered element, and $R_{E,sample}$ and $R_{E,std}$ are the isotope ratios of the element E in the sample and the corresponding standard, respectively. The reference values for the in-house ATR and METO isotope standards used in this study are provided in Table 1. Carbon and nitrogen isotope ratios of these in-house pesticide standards were determined by IRMS (Isoprime 100, Micromass) coupled to an elemental analyzer (EA, Vario MicroCube, Elementar Americas, Ronkonkoma, NY, USA). For carbon, two international reference materials (NBS19, $\delta^{13}C = -28.73 \pm 0.06$‰ and LSVEC $\delta^{13}C = -11.85 \pm 0.04$‰) were used to normalize the results on the NBS19-LSVEC scale. For nitrogen, three international reference materials were used: USGS61 ($\delta^{15}N = -2.87 \pm 0.04$‰), USGS73 ($\delta^{15}N = -5.21 \pm 0.05$‰) and USGS64 ($\delta^{15}N = +1.76 \pm 0.06$‰). For carbon and nitrogen, an additional reference material (DORM2, shark tissue, $\delta^{13}C = -17.04 \pm 0.11$‰ and $\delta^{15}N = 6.3 \pm 0.06$‰) was analyzed as an unknown to assess the exactness of the normalization. Chlorine isotope ratios of the two compound-specific chlorine standards used in this study were determined by GC-MC-ICP-MS, as explained elsewhere (Lihl et al., 2019). For C, N and Cl isotope analyses, 1 mg/mL standard stock solutions were prepared in ethyl acetate. Standards used for Cl isotope analyses were diluted in ethyl acetate to a final concentration comprised between 5 and 20 mg/L. For carbon and nitrogen isotope analyses, standards were diluted in ethyl acetate to final concentrations ranging between 30 and 800 mg/L.

The fractionation factors (ε_C, ε_{Cl} and ε_N) were determined according to the Rayleigh equation (Rayleigh, 1896):

$$\ln\left(\frac{\delta E_t + 1}{\delta E_0 + 1}\right) = \varepsilon_E \times \ln f \quad (2)$$

where δE_0 and δE_t are the isotope values of element E at the beginning of the reaction and at any time t, respectively, and f is the remaining fraction of substrate at time t. Errors given for ε values correspond to the 95% CI of the York regression in Rayleigh plots, to take into account measurement errors in both X (concentrations) and Y axes (isotope values) (Ojeda et al., 2019).

To distinguish between different degradation pathways, a dual isotope diagram or 2D-isotope plot, representing one element as a function of the other, is usually more useful than a Rayleigh plot. Dual-element isotope fractionation patterns were characterized by the slope Λ of the York regression in a 2D-isotope plot:

$$\Lambda_{C/Cl} = \frac{\Delta\delta^{13}C}{\Delta\delta^{37}Cl}; \quad \Lambda_{N/C} = \frac{\Delta\delta^{15}N}{\Delta\delta^{13}C}; \quad \Lambda_{N/Cl} = \frac{\Delta\delta^{15}N}{\Delta\delta^{37}Cl} \quad (3)$$

Uncertainties given for Λ values correspond to the 95% CI. Regressions were done in R using the 'bfsl' package. Statistical differences between different experimental conditions and with previously reported Λ and ε values were assessed using statistical two-tailed z-score tests (Ojeda et al., 2019). Differences were considered statistically significant at the $\alpha = 0.05$ confidence level. Significance of regressions was determined by a Student test ($\alpha = 0.05$). Grubbs' tests were used to detect outliers in datasets ($\alpha = 0.05$).

3. Results and discussion

3.1. Kinetics and transformation pathways

ATR and METO photodegradation followed pseudo first-order kinetics. pH values remained stable throughout the reactions (data not shown) and controls showed no sign of degradation (Fig. S2). METO generally reacted faster than ATR, with half-lives of 39.0 and 7.4 days for direct and indirect photodegradation of ATR, respectively, and 24.6 and 4.2 days for direct and indirect photodegradation of METO, respectively (Table S2). Indirect photodegradation was faster than direct photodegradation for both compounds due to the hydroxyl radical emission from nitrate in addition of direct photodegradation that was occurring in both experiments. Half-lives in this study were within the same order of magnitude (ATR and METO indirect) or one order of magnitude higher (ATR and METO direct) than previously reported kinetics under similar conditions, i.e., experiments with simulated or natural sunlight, including for direct photodegradation, and without organic matter (Drouin et al., 2021; Torrents et al., 1997; Dimou et al., 2005; Gutowski et al., 2015a; Kochany et al., 1994; Konstantinou et al., 2001; Wilson et al., 2000; Wu et al., 2021). Slightly longer half-lives in our experiments can be explained by a combination of i) higher initial concentrations of pesticides (20 mg/L for ATR and 50 mg/L for METO), required to be able to perform multi-element CSIA at an advanced stage of degradation, and ii) by lower nitrate concentration compared to other studies (Drouin et al., 2021; Torrents et al., 1997). Another explanation for longer half-lives observed during direct photodegradation lies in the lamp spectrum that was used. Hensen et al. (2019) have shown that minimal spectral differences between different irradiation source setups can have strong impact on degradation kinetics of three pesticides with limited sunlight absorption. In this setup there was no emission below 295 nm, whereas xenon lamps typically emit below these values with a cut-off at 290 nm, 270 nm or even below depending on the study. This makes emissions in this study very close to solar radiation (atmospheric UV cutoff is around 290–296 nm at earth surface (Hirt et al., 1960)), but

a significant part of the UVB spectrum (280–315 nm) was excluded, which restricts further the spectral overlap for ATR and METO that do not significantly absorb radiations above 320 nm (Cessna et al., 2008; Feigenbrugel et al., 2005).

The same transformation products (TPs) were detected during direct and indirect photodegradation of ATR, but in different proportions over the course of the experiments (Fig. 1). ATROH was the main TP during direct photodegradation representing 62% of quantified TPs at about 50% degradation, followed by DEA (21% at 50% degradation), DIAOH (12% at 50%) and DIA (5% at 50%). ATROH represented only 6% of the quantified TPs at 50% degradation during indirect photodegradation, while the main TPs were DEA (42% at 50%) and DEDIA (30% at 50%) followed by DIA (21% at 50%). ATROH was further degraded in both direct and indirect photodegradation, as well as DEA, DIA, DIAOH and DEDIA during indirect photodegradation. The dominance of ATROH during direct photodegradation (simulated sunlight and UV light) and dealkylated TPs during indirect photodegradation has been observed before (Hartenbach et al., 2008; Cessna et al., 2008). On the other hand, other studies have detected only traces of ATROH during direct photodegradation (Drouin et al., 2021; Marchetti et al., 2013; Rejto et al., 1983).

Fig. 1 shows that i) most of the quantified TPs were further degraded, and that ii) mass balances did not reach 100% (quantified TPs accounted for over 90% of all produced TPs until about 40% degradation for direct photodegradation and 20% degradation for indirect photodegradation and their concentrations subsequently decreased). Suspect-screening allowed the detection of five additional TPs: 6-amino-4-acetamido-2-chloro-*s*-triazine (CDAT, major TP for indirect photodegradation, minor for direct photodegradation, see Fig. S3), deethylhydroxyatrazine (DEAOH, major TP for both conditions, see Fig. S3), and 4-acetamido-2-chloro-6-isopropylamino-*s*-triazine (CDIT minor TP for both conditions)

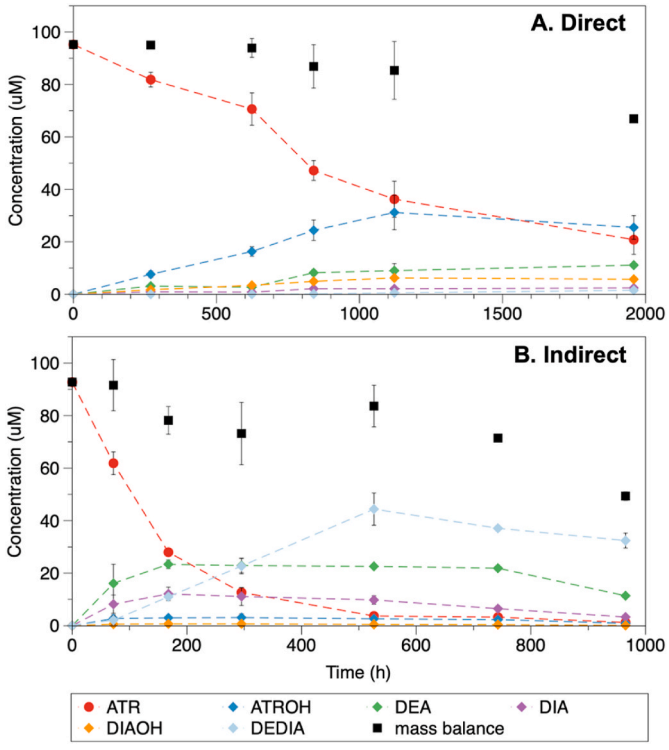

Fig. 1. Concentration of ATR (red dots) and several transformation products during direct (A) and indirect (B) photodegradation. Error bars stand for the standard deviation of concentrations in triplicate experiments. Black squares represent the sum of these transformation products. DEA: deethylatrazine; DIA: deisopropylatrazine, DEDIA: deethyldeisopropylatrazine, DIAOH: deisopropylhydroxyatrazine and ATROH: 2-hydroxy-atrazine.

that were detected in both experiments; ammelide and 4-acetamido-2-chloro-6-ethylamino-*s*-triazine (CDET) were minor TPs detected during indirect photodegradation only. Spectra and retention times for each of these additional TPs are provided in Figs. S4 and S5. Another TP that could correspond to ammeline was also detected but its retention time did not match the one from the standard compound, so it was not further considered. All of these additional TPs were previously described in literature (Torrents et al., 1997; Cessna et al., 2008).

A complete picture of primary and secondary TPs detected for ATR is shown in Fig. 2. Direct and indirect photodegradation of ATR lead to the formation of the same five primary TPs whose relative abundance depended on experimental conditions (a sixth TP, CDET, was exclusive to indirect photodegradation). The fact that ATROH was the main TP during direct photodegradation under simulated sunlight indicates that dechlorination followed by hydroxylation was a major transformation pathway under these conditions. The major transformation pathways during indirect photodegradation were *N*-ethyl oxidation and *N*-isopropyl dealkylation, leading to the formation of DEA and DIA, respectively. Direct photodegradation generally leads to photoproducts that had lost their Cl atom, while most TPs in indirect photodegradation still contain the Cl atom. The preferential formation of DEA over DIA during direct and especially indirect photodegradation with nitrate (Fig. 2) has been reported before and is probably due to sterical hindrance at the *N*-isopropyl group, as well as a weaker dissociation energy associated to the cleavage of N–C bond in the *N*-ethyl group compared to the *N*-isopropyl group (Drouin et al., 2021; Torrents et al., 1997; Marchetti et al., 2013; Rejto et al., 1983).

No TPs were detected during direct and indirect photodegradation of METO (quantified TPs and suspect-screening), except for trace amounts of METOH (<LOQ), indicating that this TP was further degraded along the course of the reaction (Fig. S6). It is possible that TPs were too polar to be retained by the column used for both quantification and suspect-screening (reverse-phase Agilent Zorbax Eclipse Plus C18), although previous studies on METO photodegradation successfully detected and quantified TPs with similar stationary phases (Drouin et al., 2021; Nicol et al., 2015) or even by GC-MS (Dimou et al., 2005; Coffinet et al., 2012). Our results partly corroborate those from Drouin et al. (2021) who did not detect TPs for indirect photodegradation of METO in the presence of nitrate, and who explained this by the non-selectivity of hydroxyl radicals, reacting fast with TPs as they were produced. They also hypothesized that METOH was not detected during direct photodegradation under simulated sunlight because it was readily degraded, which was confirmed in this study. However, they measured substantial amounts of METO-OA during direct photodegradation (simulated sunlight), which was not the case here. Previous studies have also reported the formation of HMETO during direct photodegradation under simulated sunlight and in the presence of nitrate (Dimou et al., 2005; Gutowski et al., 2015a, 2015b; Kochany et al., 1994). Most of the previously reported TPs, whether METOH, METO-OA or TPs formed with UV light have in common the loss of the chlorine atom, suggesting that the C–Cl bond cleavage is the first step of the process. Indeed, photodegradation of METO has been found to proceed through several routes including a C–Cl bond cleavage, including dechlorination, hydroxylation, and dehydrochlorination followed by cyclization (Dimou et al., 2005; Kochany et al., 1994; Katagi, 2018).

3.2. Compound specific Isotope analysis (CSIA)

3.2.1. C, N and Cl isotope fractionation associated to the photodegradation of atrazine

Direct and indirect photodegradation of ATR caused a normal isotope effect for carbon ($\varepsilon_C = -4.6 \pm 1.0$ ‰, and $\varepsilon_C = -1.4 \pm 0.2$ ‰, respectively) and nitrogen ($\varepsilon_N = -4.4 \pm 0.8$ ‰, and $\varepsilon_N = -0.6 \pm 0.2$ ‰, respectively), while a strong inverse isotope effect was observed for chlorine ($\varepsilon_{Cl} = 6.9 \pm 3.3$ ‰, and $\varepsilon_{Cl} = 2.3 \pm 1.2$ ‰, respectively, see Table 2 and Fig. 3). C–Cl and N–C dual isotope slopes were significantly

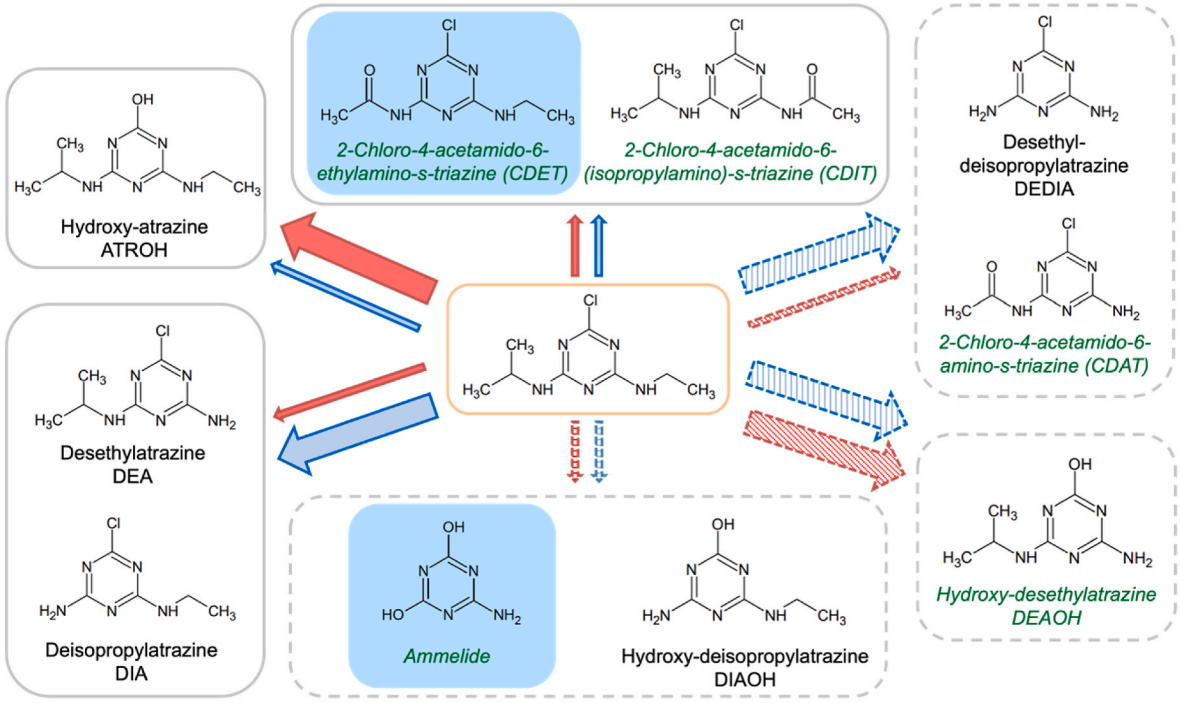

Fig. 2. Detected transformation products of ATR during direct (red) and indirect (blue) photodegradation. Bigger arrows stand for dominant TPs while the thinner ones represent minor TPs. Dashed boxes and arrows indicate secondary TPs. TPs detected during indirect photodegradation only are shown in a blue background. Green italic labels indicate TPs identified during suspect-screening.

Table 2
Carbon, chlorine and nitrogen isotope fractionations (ε_C, ε_{Cl} ε_N) and 2D-isotope slopes ($\Lambda_{C/Cl}$, $\Lambda_{N/C}$, and $\Lambda_{N/Cl}$) for direct and indirect photodegradation of ATR and METO. ε and Λ values were calculated by the York regression and uncertainty is shown as the 95% confidence interval (95% CI). When differences between direct and indirect photodegradation were not significant ($p > 0.05$), data were merged to derive combined ε and Λ values. n.s. = not significant.

Compound	Experiment	ε_C (‰) ±95% CI	ε_{Cl} (‰) ±95% CI	ε_N (‰) ±95% CI	$\Lambda_{C/Cl}$ ±95% CI	$\Lambda_{N/C}$ ±95% CI	$\Lambda_{N/Cl}$ ±95% CI
ATR	Direct photodeg.	−4.6 ± 1.0	6.9 ± 3.3	−4.4 ± 0.8	−0.49 ± 0.17	1.08 ± 0.31	−0.68 ± 0.44
	Indirect photodeg.	−1.4 ± 0.2	2.3 ± 1.2	−0.6 ± 0.2	−0.31 ± 0.10	0.40 ± 0.23	n.s.
	Combined	–	–	–	–	–	−0.87 ± 0.33
METO	Direct photodeg.	−1.2 ± 0.3	−2.2 ± 1.6	n.s.	0.48 ± 0.25	n.s.	n.s.
	Indirect photodeg.	−0.4 ± 0.1	−1.1 ± 1.1	−1.7 ± 1.3	0.37 ± 0.30	n.s.	n.s.
	Combined	–	−1.0 ± 0.7	–	0.46 ± 0.19	n.s.	1.0 ± 0.8

different between direct and indirect photodegradation, but not N–Cl dual isotope slopes, hence data from both experiments were merged (Table 2). For both ATR and METO, a comparison between ordinary linear regression and York regression for epsilon and lambda determination is provided in Tables S3 and S4. Cl isotope values were not corrected for the presence of two ^{13}C atoms, as corrected values would have been within the uncertainty range (Ponsin et al., 2019).

Isotope fractionation was systematically higher during direct compared to indirect photodegradation. This higher isotope fractionation has been observed before for several micropollutants, including ATR and METO (Zhang et al., 2014; Knossow et al., 2020; Hartenbach et al., 2008; Drouin et al., 2021). Inverse N isotope effects during direct photodegradation of organic contaminants have also been reported, including for ATR (Liu et al., 2024; Hartenbach et al., 2008; Drouin et al., 2021; Ratti et al., 2015), while a normal isotope effect was measured in this study. However, experimental conditions were different as direct photodegradation was done with shorter wavelengths in these studies and the amount of energy received was much higher than under simulated sunlight. Only one study looked at isotope fractionation during direct photodegradation under simulated sunlight, which led to insignificant C and N isotope fractionation for ATR (Drouin et al., 2021). The authors explained this result by various co-occurring reactions caused by the generation of diverse excited triplet states by the Xe lamp leading to compensating C and N isotope fractionation.

Direct photodegradation has been hypothesized to proceed via excitation of ATR followed by dechlorination and hydroxylation (Torrents et al., 1997; Katagi, 2018) and TPs detected during the reaction indicated this was the main transformation pathway in this study. The strong normal isotope effect observed for C is consistent with a hydrolysis step and C isotope fractionation is identical to previously reported values measured during abiotic hydrolysis of ATR, where ATROH was also the main TP ($\varepsilon_C = -5.6 \pm 0.8$ ‰, (Masbou et al., 2018), $\varepsilon_C = -5.6 \pm 0.1$ ‰ (Meyer et al., 2008), $\varepsilon_C = -4.0 \pm 3.3$ ‰ (Torrentó et al., 2021)). The proposed mechanism was a SN_2 nucleophilic substitution that also caused a normal isotope effect for N during alkaline hydrolysis (Torrentó et al., 2021), which is a secondary isotope effect as N atoms are present in the aromatic π-system only and are not directly involved in the reaction. Interestingly, the C–N slope obtained for direct photodegradation under simulated sunlight in this study is identical to the one obtained for direct photodegradation under UV light (λ = 254 nm) by Hartenbach et al. (2008), although the isotope effect for C and N are opposite (Fig. S7 and Table S5). This would not affect process identification during field studies, as the atmospheric cutoff around 290 nm would prevent shorter wavelengths to reach the ground. In cases

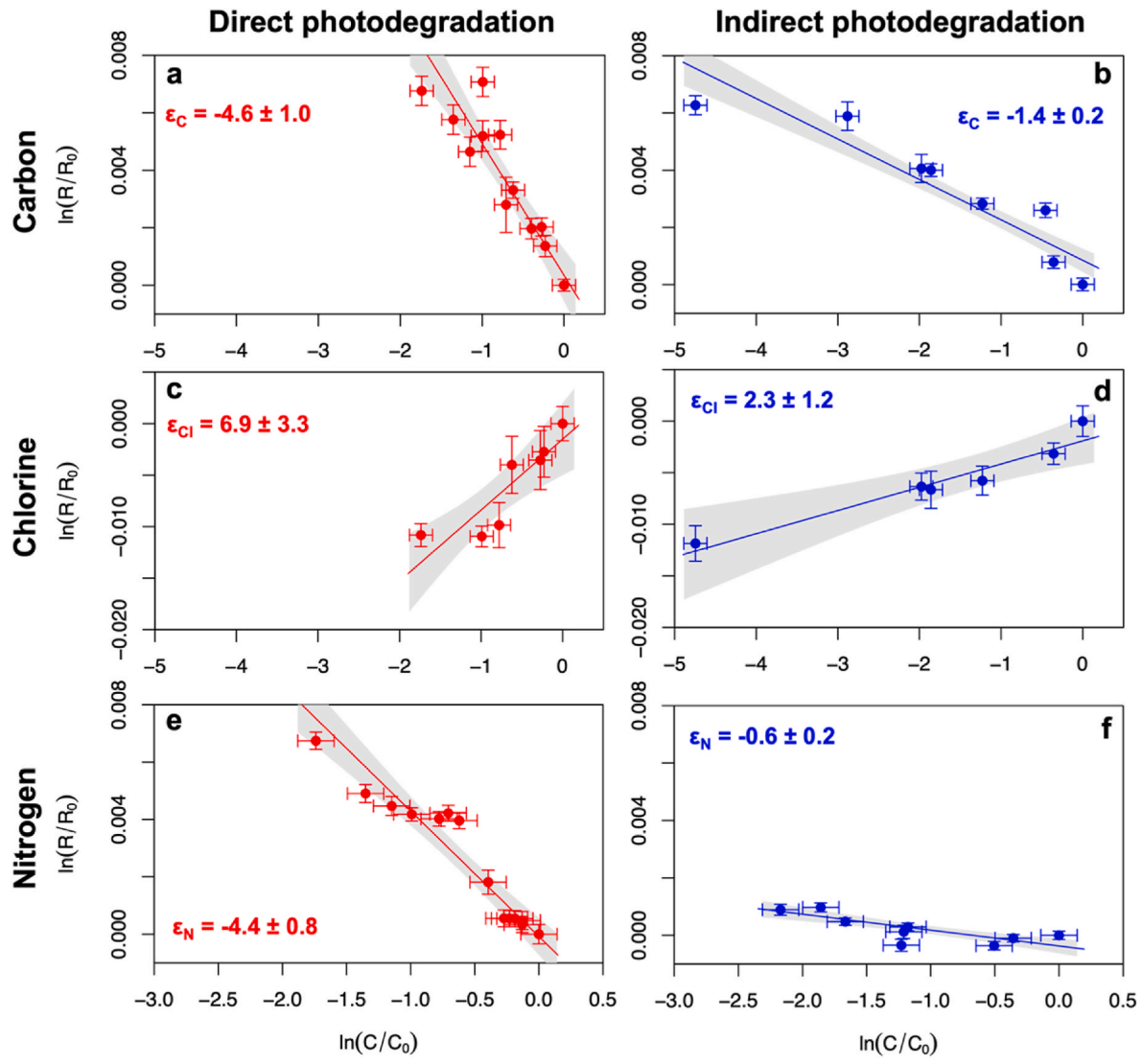

Fig. 3. Logarithmic plots according to the Rayleigh equation for C, Cl and N isotopes during direct and indirect photodegradation of ATR. Error bars show the uncertainty calculated by error propagation (for both concentration and isotope measurements). Solid lines represent York regressions with 95% CI (grey areas).

where the λ value is identical despite opposite isotope effects, the isotope value of the source has to be known to be able to tease apart processes.

Although the amplitude of fractionation factors for C and N isotopes was different between i) indirect photodegradation in this study and that of Hartenbach et al. (2008) on one hand ($\varepsilon_C = -0.5 \pm 0.2$ ‰ and $\varepsilon_N = -0.3 \pm 0.1$ ‰), and ii) this study and oxidative dealkylation catalyzed by cytochrome P450 enzyme on the other hand ((Meyer et al., 2014), $\varepsilon_C = -1.4 \pm 0.3$ ‰ and $\varepsilon_N = -0.3 \pm 0.1$ ‰), C–N dual isotope slopes were undistinguishable for the three experiments (Fig. S7 and Table S5). This result points to the same underlying mechanism: H abstraction from N–H and C–H bonds at the *N*-ethyl (DEA) or *N*-isopropyl (DIA) group respectively, which leads to a normal isotope effect for C and N (Hartenbach et al., 2008; Meyer et al., 2014). Hartenbach et al. (2008) additionally found undistinguishable C–N slopes for indirect photodegradation with DOM or with OH radicals generated by H_2O_2 (and with indirect photodegradation in this study, Table S5), suggesting that the reaction mechanism was the same with the two photooxidants. Drouin et al. (2021) also reported similar fractionation patterns for indirect photodegradation in the presence of nitrate or nitrate + DOM, and they concluded that a reaction with OH radicals generated by nitrate was the dominant process for indirect photodegradation in natural waters containing nitrate, even in the presence of DOM. However, they measured contrasting isotope fractionation compared to this study and Hartenbach's: insignificant isotope fractionation for C, and an inverse isotope effect for N during indirect photodegradation with nitrate ($\varepsilon_N = 0.7 \pm 0.3$ ‰) or nitrate + DOM ($\varepsilon_N = 0.9 \pm 0.6$ ‰), although DEA and DIA were also the main TPs formed during the reaction. Accordingly, their C–N dual isotope slope was also quite different ($\Lambda_{C/N} = 6.6 \pm 2.2$, Fig. S7). Differences and similarities observed between these three studies could be due to the emission range of the xenon lamps: cut-offs were all different, and it has been shown that small differences in emission ranges have consequences on degradation pathways, hence on isotope fractionation (Hensen et al., 2019). Our cut-off at 295 nm allowed less UVB than the one used by Drouin et al. (270 nm).

Surprisingly, a strong inverse isotope effect was measured for Cl under both conditions, especially for direct photodegradation ($\varepsilon_{Cl} = 6.9 \pm 3.3$ ‰, and $\varepsilon_{Cl} = 2.3 \pm 1.2$ ‰ for indirect photodegradation). This is, to the best of our knowledge, the first report of an inverse Cl isotope effect measured during the transformation of an organic compound. Magnetic interactions between spin carrying nuclei and unpaired electrons of excited ATR radicals leading to magnetic isotope effects (MIE) have been invoked to explain the inverse isotope effect measured for C and/or N during direct photodegradation of ATR (Hartenbach et al.,

2008; Drouin et al., 2021; Buchachenko, 1995), bromoxynil (Knossow et al., 2020) and chloroanilines (Ratti et al., 2015). For example, molecules containing a light isotope at the reactive bond tend to recombine back from singlet states to their original state while molecules containing the heavy isotope undergo conversion to a triplet state and tend to hydrolyze, leading to an inverse isotope effect (Hartenbach et al., 2008). A strong inverse isotope effect has been reported previously for bromine during direct photodegradation (UV light) of bromophenols (Zakon et al., 2013). This isotope effect was also, at least partially, associated to a MIE: although both ^{79}Br and ^{81}Br share the same spin, they have slightly different nuclear moments, which could affect the rate of the spin conversion affecting both isotopes and lead to the observed inverse isotope effect. Unless mass-dependent kinetic isotope effects, mass-independent MIEs usually do not appear during rate-limiting steps, and their sign depends on the direction of the spin conversion (Buchachenko, 1995). ^{35}Cl and ^{37}Cl also share the same spin (spin 3/2), but display a different nuclear moment (0.8218 and 0.6841 in units of the nuclear magneton, respectively (Stone, 2014)), which could lead to the inverse isotope effect observed in this study. Alternatively, excited singlet and triplet states of ATR can return to the ground-state via different photophysical processes that could be responsible for the observed isotope fractionation for Cl (Oliva et al., 2005). The relevance of these effects for the direct photodegradation of ATR would require further study.

3.2.2. *C, N and Cl isotope fractionation associated to the photodegradation of metolachlor*

Direct and indirect photodegradation of METO caused a normal isotope effect for carbon ($\varepsilon_C = -1.2 \pm 0.3$ ‰, and $\varepsilon_C = -0.4 \pm 0.1$ ‰, respectively), chlorine ($\varepsilon_{Cl} = -2.2 \pm 1.6$ ‰, and $\varepsilon_{Cl} = -1.1 \pm 1.1$ ‰, respectively), and nitrogen (insignificant fractionation for direct photodegradation, $\varepsilon_N = -1.7 \pm 1.3$ ‰ for indirect photodegradation, Table 2 and Fig. 4). N–Cl and C–Cl dual isotope slopes were not significantly different between both conditions; hence data were merged (Fig. S8). As the maximum measured shift in δ^{13}C was +3.5‰ during experiments, chlorine isotope values for METO were not corrected for the presence of two ^{13}C atoms (Ponsin et al., 2019).

Isotope fractionation was systematically higher during direct compared to indirect photodegradation, although to a lesser extent than for ATR. Isotope fractionation for C and N during indirect

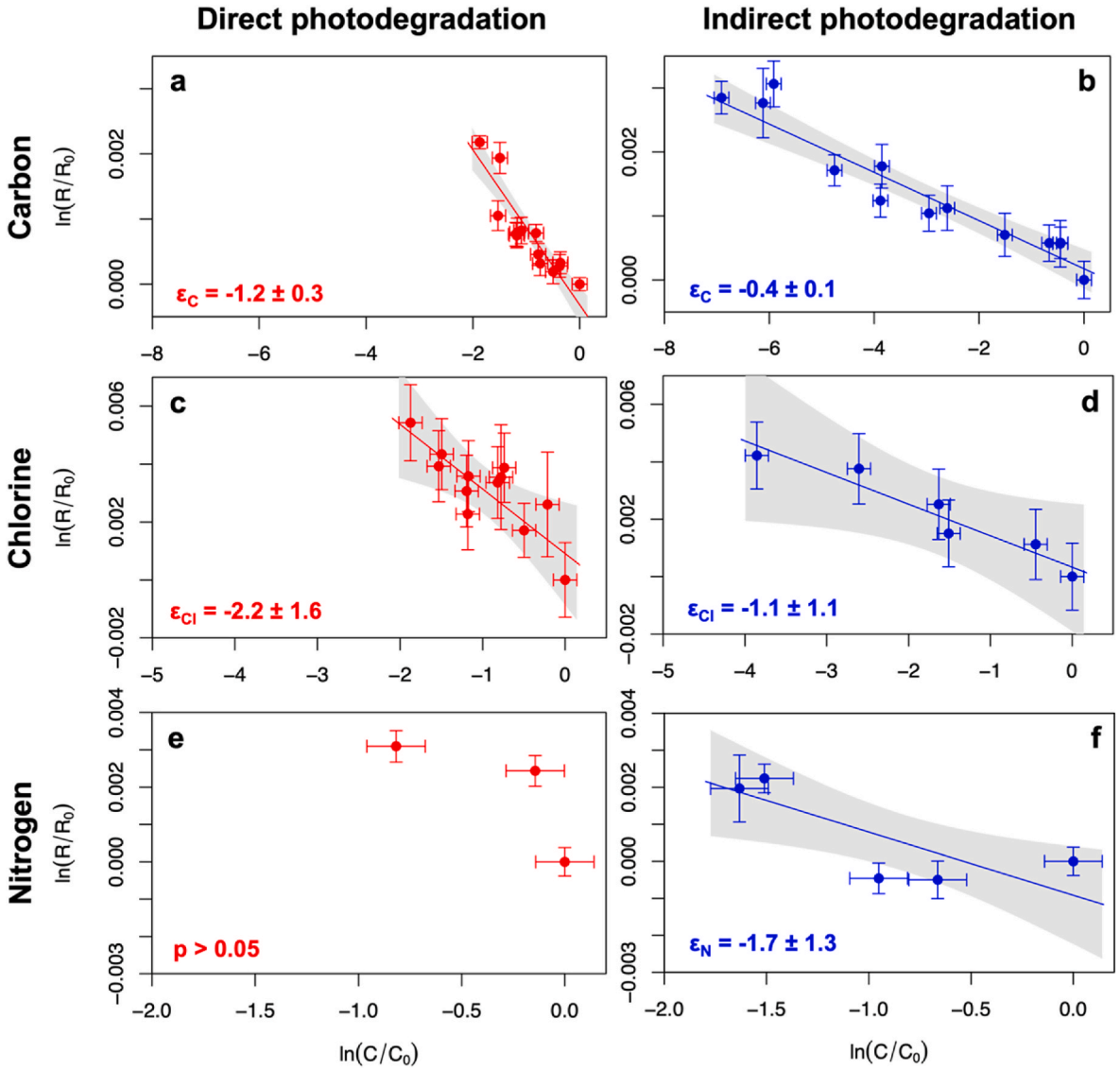

Fig. 4. Logarithmic plots according to the Rayleigh equation for C, Cl and N isotopes during direct and indirect photodegradation of METO. Error bars show the uncertainty calculated by error propagation (for both concentration and isotope measurements). Solid lines represent York regressions with 95% CI (grey areas). Regression lines are only shown when $p < 0.05$.

photodegradation with nitrate are similar to those reported by Drouin et al. (2021), who also failed to detect TPs. However, C and N isotope fractionation were insignificant during direct photodegradation in their study, while we observed a normal isotope effect for both elements. As for ATR, this difference in reactivity could be linked to different emission ranges from the Xe lamps. A comparison with the only study reporting Cl isotope data for METO (degradation in soils, and during acidic and alkaline hydrolysis (Torrentó et al., 2021)), shows that all these processes have undistinguishable C–Cl dual isotope slopes (Fig. 5 and Table S6). Detection of METO OA and METO ESA during biodegradation in soils and METOH during acidic and alkaline hydrolysis pointed to a C–Cl bond breakage as the rate-limiting step (SN_2 nucleophilic substitution (Torrentó et al., 2021),). It seems likely that the same mechanism was responsible for METO degradation in this study, although the lack of TPs (except for traces of METOH) makes it challenging to confirm. Previous studies about alkaline hydrolysis of METO reported no N isotope fractionation (Torrentó et al., 2021), or a normal effect similar to the one measured here ($\varepsilon_N = -2.0 \pm 1.3$ ‰ (Masbou et al., 2018),). As SN_2 nucleophilic substitution is not expected to induce a primary N isotope fractionation for METO, this fractionation would be associated to a secondary isotope effect.

A normal isotope effect was observed for METO, which contrasted with the inverse effect measured for ATR. This difference in the direction of isotope fractionation could be explained by the position of the Cl atom in the molecule (connected directly to the aromatic ring in ATR; connected to an aliphatic carbon in METO), and to the difference in excitation of aliphatic versus aromatic systems. Although the reaction mechanism seems to be similar to degradation processes previously studied for METO, the fractionation factor for Cl is much smaller ($\varepsilon_{Cl} = -1.0 \pm 0.7$ ‰ for combined experiments, versus $\varepsilon_{Cl} = -6.5 \pm 0.7$ ‰ for hydrolysis and $\varepsilon_{Cl} = -5.0 \pm 2.3$ ‰ for biodegradation in soils (Torrentó et al., 2021),). This suggests a masking effect from non-fractionating steps (Elsner, 2010), also affecting C fractionation ($\varepsilon_C = -1.2 \pm 0.3$ ‰ for direct photodegradation, versus $\varepsilon_C = -3.9 \pm 1.3$ ‰ for alkaline hydrolysis (Torrentó et al., 2021)), as the C–Cl dual isotope slope is undistinguishable from slopes associated to a C–Cl bond breakage by SN_2 nucleophilic substitution (Fig. 5 and Table S6). This low isotope sensitivity could be due to photophysical processes driving excitation and relaxation of METO molecules, although this hypothesis would require further testing.

3.2.3. *Multi-elements CSIA: a tool to track photodegradation of atrazine and metolachlor in water?*

Photodegradation can be a substantial process contributing to pesticide attenuation in surface water, especially in systems with longer residence times such as agricultural ponds (Imfeld et al., 2021), wetlands (Zeng et al., 2013), lakes (Huntscha et al., 2008) and some rivers (Fono et al., 2006). As different degradation processes can lead to the formation of the same TPs for both ATR and METO, these TPs cannot be used for process identification in field studies. For example, HATR, DEA and DIA are produced by photodegradation, but also by abiotic and biotic hydrolysis (Marchetti et al., 2013; Lihl et al., 2020), which are processes likely to happen in surface water concomitantly to photodegradation.

Dual isotope slopes obtained in this study for ATR and METO (C–N, Cl–C and Cl–N, Table 2) were compared to data from literature for processes relevant to natural attenuation in environmental conditions to assess whether different degradation processes could be distinguished (Fig. 5, Figs. S7 and S8). Statistical comparisons of the regression data (z-score tests) are shown in Tables S5 and S6. For ATR, C and N data only do not allow to distinguish between indirect photodegradation ($\Lambda_{C/N} = 0.4 \pm 0.2$, this study and (Hartenbach et al., 2008)) and oxidative dealkylation ($\Lambda_{C/N} = 0.5 \pm 0.1$ (Meyer et al., 2014; Lihl et al., 2020),), which are both relevant processes in surface water. These two processes can be teased apart when considering Cl–C plots ($\Lambda_{Cl/C} = -0.3 \pm 0.1$ and $\Lambda_{Cl/C} = 0.6 \pm 0.1$, respectively, Fig. 5) and Cl–N plots ($\Lambda_{Cl/N} = -0.8 \pm 0.3$ and $\Lambda_{Cl/N} = 0.4 \pm 0.2$, respectively, Fig. S7). The slope for indirect photodegradation in C–Cl dual isotope plots also had the smallest absolute value, which means that even for limited degradation, it could still show a depletion in heavy isotopes for Cl. Indirect photodegradation of ATR in surface water could potentially be identified with Cl isotope only, provided that the signature of applied ATR is known (Masbou et al., 2024). A complete determination of the relative contribution of different pathways would still require a second element, C being the most relevant element to measure.

There is limited data about isotope fractionation associated with different degradation processes of METO compared to ATR. Unfortunately, Cl–C slopes do not allow to distinguish between

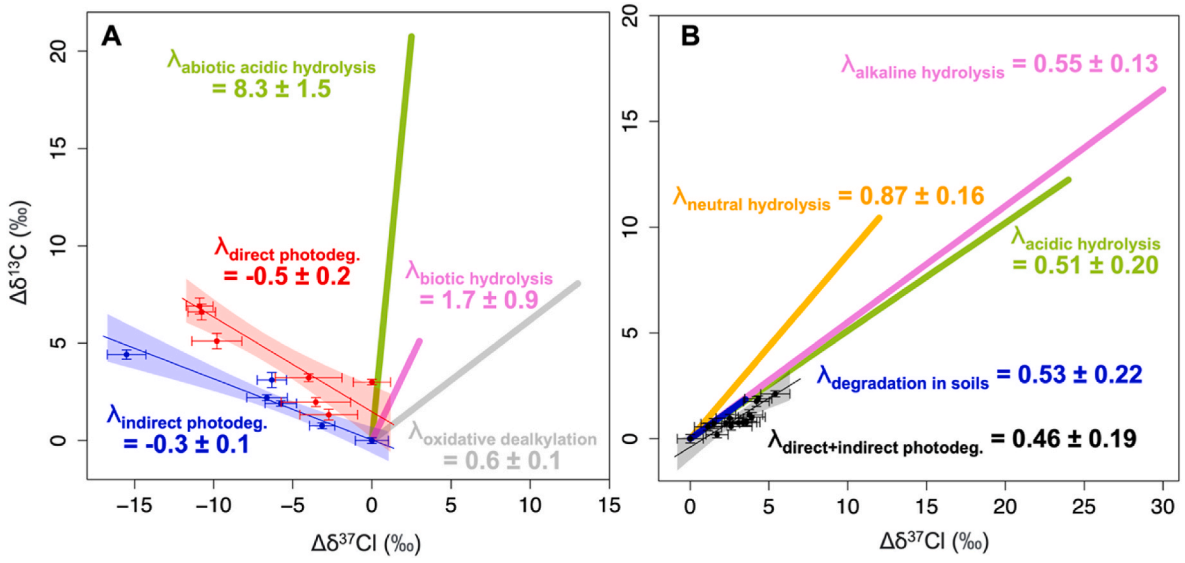

Fig. 5. Dual Cl and C isotope plots obtained for A) atrazine, and B) metolachlor for different degradation processes. Uncertainties for photodegradation are shown as 95% CI (this study). Data for direct and indirect photodegradation of METO were merged as they were not significantly different (two-tailed z-score test). Slopes obtained in this study were compared for ATR to trends obtained for oxidative dealkylation and biotic hydrolysis (Lihl et al., 2020), and abiotic acidic hydrolysis (Torrentó et al., 2021). All regressions were significantly different. For METO, slopes were compared to those measured for degradation in soils, acidic, alkaline and neutral abiotic hydrolysis (Torrentó et al., 2021). Data were not significantly different ($\alpha = 0.05$), except for neutral hydrolysis versus all other processes.

photodegradation, biodegradation and abiotic hydrolysis, whether alkaline or acidic (Fig. 5). A distinction can be made between photodegradation and acidic hydrolysis in Cl–N plots, although regressions are associated with a high uncertainty and should be interpreted accordingly (Fig. S8). However, N isotopes are more challenging to measure in METO that contains only one N atom. The differences in C–N dual isotope slopes for the different degradation pathways were not statistically significant. As mentioned before, undistinguishable dual isotope slopes point towards the same mechanism for all these processes, i.e. a C–Cl bond cleavage associated to a SN_2 type nucleophilic substitution.

4. Conclusions

This study provides a 3D-isotope (C, N, Cl) approach for direct and indirect photodegradation with OH radicals in the presence of nitrate of two frequently detected herbicides in surface water, atrazine and metolachlor. C and N fractionation patterns provide new insights into contrasting results from previous studies (Hartenbach et al., 2008; Drouin et al., 2021), and reinforces previous observations about the sensitivity of transformation pathways and fractionation patterns to irradiation sources. Cl isotopes for ATR showed an unexpected and strong inverse isotope effect during both direct and indirect photodegradation, which provides a unique pattern to tease apart photodegradation from other processes relevant in surface water such as biodegradation (biotic hydrolysis and oxidative dealkylation) and abiotic hydrolysis. The extent of Cl isotope fractionation also makes Cl a sensitive indicator of degradation for ATR and underlines the benefit of including Cl isotope analysis in future field studies. For METO the C–Cl fractionation pattern is identical to other processes such as hydrolysis and biodegradation but with limited amplitude, pointing to the same reaction mechanism with masking effects. OH radicals are also assumed to play a major role during indirect photodegradation in the presence of DOM (Min et al., 2023), although the complexity of DOM and the diversity of its effects on photodegradation points to site-specific studies to determine associated isotope fractionation. Recent developments in SPE-CSIA for large volume environmental water samples (Torrentó et al., 2019), in the use of Polar Organic Chemical Integrative Sampler (POCIS) associated to CSIA (Suchana et al., 2024), and on sample clean-up approaches for CSIA (Glöckler et al., 2023) represent major promises to bring this approach to the field, at environmental concentrations, for a diversity of micropollutants.

CRediT authorship contribution statement

Matias Levesque-Vargas: Writing – original draft, Visualization, Investigation, Formal analysis, Conceptualization. **Leanne Ohlund:** Writing – review & editing, Resources, Methodology. **Lekha Sleno:** Writing – review & editing, Resources, Methodology. **Yves Gélinas:** Writing – review & editing, Resources, Methodology. **Patrick Höhener:** Writing – review & editing, Resources, Methodology, Formal analysis. **Violaine Ponsin:** Writing – review & editing, Supervision, Resources, Project administration, Funding acquisition, Conceptualization.

Supporting information

Additional information on the experimental setup, analytical methods, degradation kinetics, transformation products, and isotope data for atrazine and metolachlor.

Declaration of competing interest

The authors declare that they have no known competing financial interests or personal relationships that could have appeared to influence the work reported in this paper.

Acknowledgments

This study was supported by the National Science and Engineering Research Council of Canada (grant RGPIN-2021-03309 to Violaine Ponsin). The authors thank Paul Del Giorgio for access to the photoreactor, Alice Parkes and Didier Gori for assistance in the laboratory, as well as Gwenaël Imfeld for N isotopes measurement in metolachlor.

Appendix A. Supplementary data

Supplementary data to this article can be found online at https://doi.org/10.1016/j.chemosphere.2024.144010.

Data availability

Data will be made available on request.

References

Aelion, C.E., Höhener, P.E., Hunkeler, D.E., Aravena, R.E., 2009. Environmental Isotopes in Biodegradation and Bioremediation. CRC Press, Boca Raton. https://doi.org/10.1201/9781420012613.

Agency, U.S.E.P., 2008. Regulatory Determinations Support Document for Selected Contaminants from the Second Drinking Water Contaminant Candidate List (CCL 2). U.S.EPA, p. 497.

Almberg, K.S., Turyk, M.E., Jones, R.M., Rankin, K., Freels, S., Stayner, L.T., 2018. Atrazine contamination of drinking water and adverse birth outcomes in community water systems with elevated atrazine in Ohio, 2006–2008. Int. J. Environ. Res. Publ. Health 15 (9), 1889–1903. https://doi.org/10.3390/ijerph15091889.

Bernstein, A., Shouakar-Stash, O., Ebert, K., Laskov, C., Hunkeler, D., Jeannottat, S., Sakaguchi-Söder, K., Laaks, J., Jochmann, M.A., Cretnik, S., Jager, J., Haderlein, S. B., Schmidt, T.C., Aravena, R., Elsner, M., 2011. Compound-specific chlorine isotope analysis: a comparison of gas chromatography/isotope ratio mass spectrometry and gas chromatography/quadrupole mass spectrometry methods in an interlaboratory study. Anal. Chem. 83 (20), 7624–7634. https://doi.org/10.1021/ac200516c.

Buchachenko, A.L., 1995. MIE versus CIE: comparative analysis of magnetic and classical isotope effects. Chem. Rev. 95 (7), 2507–2528. https://doi.org/10.1021/cr00039a009.

Cessna, A.J., 2008. Nonbiological degradation of triazine herbicides: photolysis and hydrolysis. In: Lebaron, H., McFarland, J.E., Burnside, O.C. (Eds.), The Triazine Herbicides: 50 Years Revolutionizing Agriculture. Elsevier, Amsterdam, The Netherlands, pp. 329–353.

Coffinet, S., Rifai, A., Genty, C., Souissi, Y., Bourcier, S., Sablier, M., Bouchonnet, S., 2012. Characterization of the photodegradation products of metolachlor: structural elucidation, potential toxicity and persistence. J. Mass Spectrom. 47 (12), 1582–1593. https://doi.org/10.1002/jms.3121.

Dimou, A.D., Sakkas, V.A., Albanis, T.A., 2005. Metolachlor photodegradation study in aqueous media under natural and simulated solar irradiation. J. Agric. Food Chem. 53 (3), 694–701. https://doi.org/10.1021/jf048766w.

Drouin, G., Droz, B., Leresche, F., Payraudeau, S., Masbou, J., Imfeld, G., 2021. Direct and indirect photodegradation of atrazine and S-metolachlor in agriculturally impacted surface water and associated C and N isotope fractionation. Environ. Sci. J. Integr. Environ. Res.: Process. Impacts 23, 1791–1802. https://doi.org/10.1039/D1EM00246E.

ECHA (European Chemicals Agency), 2022. Committee for Risk Assessment (RAC) Opinion proposing harmonised classification and labelling at EU level of S-metolachlor. CLH-O-0000007145-77-01/F. Adopted Available online. www.echa.europa.eu. (Accessed 2 June 2022).

Elsner, M., 2010. Stable isotope fractionation to investigate natural transformation mechanisms of organic contaminants: principles, prospects and limitations. J. Environ. Monit. 12 (11), 2005–2031. https://doi.org/10.1039/c0em00277a.

Evans, S., Campbell, C., Naidenko, O.V., 2019. Cumulative risk analysis of carcinogenic contaminants in United States drinking water. Heliyon 5 (9), e02314. https://doi.org/10.1016/j.heliyon.2019.e02314.

Feigenbrugel, V., Loew, C., Calvé, S.L., Mirabel, P., 2005. Near-UV molar absorptivities of acetone, alachlor, metolachlor, diazinon and dichlorvos in aqueous solution. J. Photochem. Photobiol. Chem. 174 (1), 76–81. https://doi.org/10.1016/j.jphotochem.2005.03.014.

Fenner, K., Canonica, S., Wackett, L.P., Elsner, M., 2013. Evaluating pesticide degradation in the environment: blind spots and emerging opportunities. Science 341 (6147), 752. https://doi.org/10.1126/science.1236281.

Fenner, K., Elsner, M., Lueders, T., McLachlan, M.S., Wackett, L.P., Zimmermann, M., Drewes, J.E., 2021. Methodological advances to study contaminant biotransformation: new prospects for understanding and reducing environmental persistence? ACS ES&T Water 1 (7), 1541–1554. https://doi.org/10.1021/acsestwater.1c00025.

Fono, L.J., Kolodziej, E.P., Sedlak, D.L., 2006. Attenuation of wastewater-derived contaminants in an effluent-dominated river. Environ. Sci. Technol. 40 (23), 7257–7262. https://doi.org/10.1021/es061308e.

Gerecke, A.C., Canonica, S., Müller, S.R., Schärer, M., Schwarzenbach, R.P., 2001. Quantification of dissolved natural organic matter (DOM) mediated phototransformation of phenylurea herbicides in lakes. Environ. Sci. Technol. 35 (19), 3915–3923. https://doi.org/10.1021/es010103x.

Glöckler, D., Wabnitz, C., Elsner, M., Bakkour, R., 2023. Avoiding interferences in advance: cyclodextrin polymers to enhance selectivity in extraction of organic micropollutants for carbon isotope analysis. Anal. Chem. 95 (20), 7839–7848. https://doi.org/10.1021/acs.analchem.2c05465.

Gutowski, L., Olsson, O., Leder, C., Kümmerer, K., 2015a. A comparative assessment of the transformation products of S-metolachlor and its commercial product Mercantor Gold® and their fate in the aquatic environment by employing a combination of experimental and in silico methods. Sci. Total Environ. 506–507, 369–379. https://doi.org/10.1016/j.scitotenv.2014.11.025.

Gutowski, L., Baginska, E., Olsson, O., Leder, C., Kümmerer, K., 2015b. Assessing the environmental fate of S-metolachlor, its commercial product Mercantor Gold® and their photoproducts using a water–sediment test and in silico methods. Chemosphere 138, 847–855. https://doi.org/10.1016/j.chemosphere.2015.08.013.

Hartenbach, A.E., Hofstetter, T.B., Tentscher, P.R., Canonica, S., Berg, M., Schwarzenbach, R.P., 2008. Carbon, hydrogen, and nitrogen isotope fractionation during light-induced transformations of atrazine. Environ. Sci. Technol. 42 (21), 7751–7756. https://doi.org/10.1021/es800356h.

Hensen, B., Olsson, O., Kümmerer, K., 2019. The role of irradiation source setups and indirect phototransformation: kinetic aspects and the formation of transformation products of weakly sunlight-absorbing pesticides. Sci. Total Environ. 695, 133808. https://doi.org/10.1016/j.scitotenv.2019.133808.

Hirt, R.C., Schmitt, R.G., Searle, N.D., Sullivan, A.P., 1960. Ultraviolet spectral energy distributions of natural sunlight and accelerated test light sources. J. Opt. Soc. Am. 50 (7), 706–713. https://doi.org/10.1364/JOSA.50.000706.

Höhener, P., Guers, D., Malleret, L., Boukaroum, O., Martin-Laurent, F., Masbou, J., Payraudeau, S., Imfeld, G., 2022. Multi-elemental compound-specific isotope analysis of pesticides for source identification and monitoring of degradation in soil: a review. Environ. Chem. Lett. 20 (6), 3927–3942. https://doi.org/10.1007/s10311-022-01489-8.

Huntscha, S., Singer, H., Canonica, S., Schwarzenbach, R.P., Fenner, K., 2008. Input dynamics and fate in surface water of the herbicide metolachlor and of its highly mobile transformation product metolachlor ESA. Environ. Sci. Technol. 42 (15), 5507–5513. https://doi.org/10.1021/es800395c.

Imfeld, G., Payraudeau, S., Tournebize, J., Sauvage, S., Macary, F., Chaumont, C., Probst, A., Sánchez-Pérez, J.-M., Bahi, A., Chaumet, B., Gilevska, T., Alexandre, H., Probst, J.-L., 2021. The role of ponds in pesticide dissipation at the agricultural catchment scale: a critical review. Water 13 (9). https://doi.org/10.3390/w13091202.

Junginger, T., Payraudeau, S., Imfeld, G., 2022. Transformation and stable isotope fractionation of the urban biocide terbutryn during biodegradation, photodegradation and abiotic hydrolysis. Chemosphere 305, 135329. https://doi.org/10.1016/j.chemosphere.2022.135329.

Katagi, T., 2018. Direct photolysis mechanism of pesticides in water. J. Pestic. Sci. 43 (2), 57–72. https://doi.org/10.1584/jpestics.D17-081.

Kim, K.-H., Kabir, E., Jahan, S.A., 2017. Exposure to pesticides and the associated human health effects. Sci. Total Environ. 575, 525–535. https://doi.org/10.1016/j.scitotenv.2016.09.009.

Knossow, N., Siebner, H., Bernstein, A., 2020. Isotope analysis method for the herbicide bromoxynil and its application to study photo-degradation processes. J. Hazard Mater., 122036 https://doi.org/10.1016/j.jhazmat.2020.122036.

Kochany, J., Maguire, R.J., 1994. Sunlight photodegradation of metolachlor in water. J. Agric. Food Chem. 42 (2), 406–412. https://doi.org/10.1021/jf00038a032.

Konstantinou, I.K., Zarkadis, A.K., Albanis, T.A., 2001. Photodegradation of selected herbicides in various natural waters and soils under environmental conditions. J. Environ. Qual. 30 (1), 121–130. https://doi.org/10.2134/jeq2001.301121x.

Lihl, C., Renpenning, J., Kümmel, S., Gelman, F., Schuerner, H., Daubmeier, M., Heckel, B., Melsbach, A., Bernstein, A., Shouakar-Stash, O., Gehre, M., Elsner, M., 2019. Towards improved accuracy in chlorine isotope analysis: synthesis routes for in-house standards and characterization via complementary mass spectrometry methods. Anal. Chem. 91 (19), 12290–12297. https://doi.org/10.1021/acs.analchem.9b02463.

Lihl, C., Heckel, B., Grzybkowska, A., Dybala-Defratyka, A., Ponsin, V., Torrentó, C., Hunkeler, D., Elsner, M., 2020. Compound-specific chlorine isotope fractionation in biodegradation of atrazine. Environ. Sci. J. Integr. Environ. Res.: Process. Impacts 22, 792–801. https://doi.org/10.1039/C9EM00503J.

Liu, Y., Mekic, M., Carena, L., Vione, D., Gligorovski, S., Zhang, G., Jin, B., 2020. Tracking photodegradation products and bond-cleavage reaction pathways of triclosan using ultra-high resolution mass spectrometry and stable carbon isotope analysis. Environ. Pollut. 264, 114673. https://doi.org/10.1016/j.envpol.2020.114673.

Liu, X., Akay, C., Köpke, J., Kümmel, S., Richnow, H.H., Imfeld, G., 2024. Direct phototransformation of sulfamethoxazole characterized by four-dimensional element compound specific isotope analysis. Environ. Sci. Technol. 58 (23), 10322–10333. https://doi.org/10.1021/acs.est.4c02666.

Mabury, S.A., Crosby, D.G., 1996. Pesticide reactivity toward hydroxyl and its relationship to field persistence. J. Agric. Food Chem. 44 (7), 1920–1924. https://doi.org/10.1021/jf950423y.

Maier, M.P., Prasse, C., Pati, S.G., Nitsche, S., Li, Z., Radke, M., Meyer, A., Hofstetter, T. B., Ternes, T.A., Elsner, M., 2016. Exploring trends of C and N isotope fractionation to trace transformation reactions of diclofenac in natural and engineered systems. Environ. Sci. Technol. 50 (20), 10933–10942. https://doi.org/10.1021/acs.est.6b02104.

Marchetti, G., Minella, M., Maurino, V., Minero, C., Vione, D., 2013. Photochemical transformation of atrazine and formation of photointermediates under conditions relevant to sunlit surface waters: laboratory measures and modelling. Water Res. 47 (16), 6211–6222. https://doi.org/10.1016/j.watres.2013.07.038.

Masbou, J., Drouin, G., Payraudeau, S., Imfeld, G., 2018. Carbon and nitrogen stable isotope fractionation during abiotic hydrolysis of pesticides. Chemosphere 213, 368–376. https://doi.org/10.1016/j.chemosphere.2018.09.056.

Masbou, J., Höhener, P., Payraudeau, S., Martin-Laurent, F., Imfeld, G., 2024. Stable isotope composition of pesticides in commercial formulations: the ISOTOPEST database. Chemosphere, 141488. https://doi.org/10.1016/j.chemosphere.2024.141488.

Meyer, A.H., Penning, H., Lowag, H., Elsner, M., 2008. Precise and accurate compound specific carbon and nitrogen isotope analysis of atrazine: critical role of combustion oven conditions. Environ. Sci. Technol. 42 (21), 7757–7763. https://doi.org/10.1021/es800534h.

Meyer, A.H., Dybala-Defratyka, A., Alaimo, P.J., Geronimo, I., Sanchez, A.D., Cramer, C. J., Elsner, M., 2014. Cytochrome P450-catalyzed dealkylation of atrazine byRhodococcussp. strain NI86/21 involves hydrogen atom transfer rather than single electron transfer. Dalton Trans. 43 (32), 12175–12186. https://doi.org/10.1039/C4DT00891J.

Min, N., Yao, J., Li, H., Chen, Z., Pang, W., Zhu, J., Kümmel, S., Schaefer, T., Herrmann, H., Richnow, H.H., 2023. Humic substance photosensitized degradation of phthalate esters characterized by 2H and 13C isotope fractionation. Environ. Sci. Technol. 57 (5), 1930–1939. https://doi.org/10.1021/acs.est.2c06783.

Montiel-León, J.M., Vo Duy, S., Munoz, G., Bouchard, M.F., Amyot, M., Sauvé, S., 2019. Quality survey and spatiotemporal variations of atrazine and desethylatrazine in drinking water in Quebec, Canada. Sci. Total Environ. 671, 578–585. https://doi.org/10.1016/j.scitotenv.2019.03.228.

Nicol, É., Genty, C., Bouchonnet, S., Bourcier, S., 2015. Structural elucidation of metolachlor photoproducts by liquid chromatography/high-resolution tandem mass spectrometry. Rapid Commun. Mass Spectrom. 29 (23), 2279–2286. https://doi.org/10.1002/rcm.7382.

Ojeda, A.S., Phillips, E., Mancini, S.A., Lollar, B.S., 2019. Sources of uncertainty in biotransformation mechanistic interpretations and remediation studies using CSIA. Anal. Chem. 91 (14), 9147–9153. https://doi.org/10.1021/acs.analchem.9b01756.

Oliva, J.M., Azenha, M.E.D.G., Burrows, H.D., Coimbra, R., Seixas de Melo, J.S., Canle L, M., Fernández, M.I., Santaballa, J.A., Serrano-Andrés, L., 2005. On the low-lying excited states of sym-triazine-based herbicides. ChemPhysChem 6 (2), 306–314. https://doi.org/10.1002/cphc.200400349.

Ponsin, V., Torrentó, C., Lihl, C., Elsner, M., Hunkeler, D., 2019. Compound-specific chlorine isotope analysis of the herbicides atrazine, acetochlor and metolachlor. Anal. Chem. 91 (22), 14290–14298. https://doi.org/10.1021/acs.analchem.9b02497.

Prieto-Espinoza, M., Malleret, L., Ravier, S., Höhener, P., 2023. A novel multi-ion evaluation scheme to determine stable chlorine isotope ratios (37Cl/35Cl) of chlordecone by LC-QTOF. J. Am. Soc. Mass Spectrom. https://doi.org/10.1021/jasms.3c00270.

Ratti, M., Canonica, S., McNeill, K., Bolotin, J., Hofstetter, T.B., 2015. Isotope fractionation associated with the photochemical dechlorination of chloroanilines. Environ. Sci. Technol. 49 (16), 9797–9806. https://doi.org/10.1021/acs.est.5b02602.

Rayleigh, L.L., 1896. Theoretical considerations respecting the separation of gases by diffusion and similar processes. London, Edinburgh Dublin Phil. Mag. J. Sci. 42 (259), 493–498. https://doi.org/10.1080/14786449608620944.

Rejto, M., Saltzman, S., Acher, A.J., Muszkat, e., 1983. Identification of sensitized photooxidation products of s-triazine herbicides in water. J. Agric. Food Chem. 31, 138–142. https://doi.org/10.1021/jf00115a033.

Renpenning, J., Horst, A., Schmidt, M., Gehre, M., 2018. Online isotope analysis of 37Cl/35Cl universally applied for semi-volatile organic compounds using GC-MC-ICPMS. J. Anal. Atomic Spectrom. 33 (2), 314–321. https://doi.org/10.1039/C7JA00404D.

Schwarzenbach, R.P., Gschwend, P.M., Imboden, D.M., 2003. Environmental Organic Chemistry, second ed. John Wiley & Sons, Inc, New-York.

Stone, N., 2014. Table of Nuclear Magnetic Dipole and Electric Quadrupole Moments. International Atomic Energy Agency.

Suchana, S., Edwards, E., Mack, E.E., Lomheim, L., Melo, N., Gavazza, S., Passeport, E., 2024. Compatibility of polar organic chemical integrative sampler (POCIS) with compound specific isotope analysis (CSIA) of substituted chlorobenzenes. Sci. Total Environ. 906, 167628. https://doi.org/10.1016/j.scitotenv.2023.167628.

Tavera-Mendoza, L., Ruby, S., Brousseau, P., Fournier, M., Cyr, D., Marcogliese, D., 2002. Response of the amphibian tadpole (Xenopus laevis) to atrazine during sexual differentiation of the testis. Environ. Toxicol. Chem. 21 (3), 527–531. https://doi.org/10.1002/etc.5620210309.

Torrentó, C., Bakkour, R., Glauser, G., Melsbach, A., Ponsin, V., Hofstetter, T.B., Elsner, M., Hunkeler, D., 2019. Solid-phase extraction method for stable isotope analysis of pesticides from large volume environmental water samples. Analyst 144 (9), 2898–2908. https://doi.org/10.1039/c9an00160c.

Torrentó, C., Ponsin, V., Lihl, C., Hofstetter, T.B., Baran, N., Elsner, M., Hunkeler, D., 2021. Triple-element compound-specific stable isotope analysis (3D-CSIA): added value of Cl isotope ratios to assess herbicide degradation. Environ. Sci. Technol. 55 (20), 13891–13901. https://doi.org/10.1021/acs.est.1c03981.

Torrents, A., Anderson, B.G., Bilboulian, S., Johnson, W.E., Hapeman, C.J., 1997. Atrazine photolysis: mechanistic investigations of direct and nitrate-mediated hydroxy radical processes and the influence of dissolved organic carbon from the chesapeake bay. Environ. Sci. Technol. 31 (5), 1476–1482. https://doi.org/10.1021/es9607289.

Vijver, M.G., Hunting, E.R., Nederstigt, T.A.P., Tamis, W.L.M., Van Den Brink, P.J., Van Bodegom, P.M., 2017. Postregistration monitoring of pesticides is urgently required to protect ecosystems. Environ. Toxicol. Chem. 36 (4), 860–865. https://doi.org/10.1002/etc.3721.

Vinyes-Nadal, M., Masbou, J., Kümmel, S., Gehre, M., Imfeld, G., Otero, N., Torrentó, C., 2024. Novel extraction methods and compound-specific isotope analysis of methoxychlor in environmental water and aquifer slurry samples. Sci. Total Environ. 931, 172858. https://doi.org/10.1016/j.scitotenv.2024.172858.

Vione, D., Das, R., Rubertelli, F., Maurino, V., Minero, C., Barbati, S., Chiron, S., 2010. Modelling the occurrence and reactivity of hydroxyl radicals in surface waters: implications for the fate of selected pesticides. Int. J. Environ. Anal. Chem. 90 (3–6), 260–275. https://doi.org/10.1080/03067310902894218.

Wilson, R.I., Mabury, S.A., 2000. Photodegradation of metolachlor: isolation, identification, and quantification of monochloroacetic acid. J. Agric. Food Chem. 48 (3), 944–950. https://doi.org/10.1021/jf990618w.

Wu, L., Yao, J., Trebse, P., Zhang, N., Richnow, H.H., 2014. Compound specific isotope analysis of organophosphorus pesticides. Chemosphere 111, 458–463. https://doi.org/10.1016/j.chemosphere.2014.04.037.

Wu, L., Chládková, B., Lechtenfeld, O.J., Lian, S., Schindelka, J., Herrmann, H., Richnow, H.H., 2018. Characterizing chemical transformation of organophosphorus compounds by 13C and 2H stable isotope analysis. Sci. Total Environ. 615, 20–28. https://doi.org/10.1016/j.scitotenv.2017.09.233.

Wu, B., Arnold, W.A., Ma, L., 2021. Photolysis of atrazine: role of triplet dissolved organic matter and limitations of sensitizers and quenchers. Water Res. 190, 116659. https://doi.org/10.1016/j.watres.2020.116659.

Zakon, Y., Halicz, L., Gelman, F., 2013. Bromine and carbon isotope effects during photolysis of brominated phenols. Environ. Sci. Technol. 47 (24), 14147–14153. https://doi.org/10.1021/es403545r.

Zeng, T., Arnold, W.A., 2013. Pesticide photolysis in prairie potholes: probing photosensitized processes. Environ. Sci. Technol. 47 (13), 6735–6745. https://doi.org/10.1021/es3030808.

Zhang, N., Bashir, S., Qin, J., Schindelka, J., Fischer, A., Nijenhuis, I., Herrmann, H., Wick, L.Y., Richnow, H.H., 2014. Compound specific stable isotope analysis (CSIA) to characterize transformation mechanisms of α-hexachlorocyclohexane. J. Hazard Mater. 280, 750–757. https://doi.org/10.1016/j.jhazmat.2014.08.046.